JOURNAL OF GEOPHYSICAL RESEARCH, VOL. 111, D14201, doi:10.1029/2005JD006892, 2006

Single scattering parameters of randomly oriented snow particles at microwave frequencies

Min-Jeong Kim[1,2,3]

Received 15 November 2005; revised 14 February 2006; accepted 24 March 2006; published 18 July 2006.

[1] To develop a generally applicable fast and accurate parameterization method for computations of single scattering parameters at microwave frequencies requires a thorough knowledge of how the ice particle shape affects the scattering parameters. This study computes single scattering parameters (scattering cross sections (C_{sca}), absorption cross sections (C_{abs}), and asymmetry factors) of various nonspherical snow particles using the discrete dipole approximation (DDA) method and the T-matrix method to examine the sensitivity of scattering parameters to snow particles at frequencies between 95 GHz and 340 GHz. Results show that $C_{sca}/\pi r_{eff}^2$, $C_{abs}/\pi r_{eff}^2$, and asymmetry factors of complex particles at a fixed size parameter $x = 2\pi r_{eff}/\lambda$ do not depend on the specific particle shapes when x is less than about 2.5. Here λ is the wavelength and r_{eff} is the radius of equal-volume ice spheres. The Mie theory may be used to compute the single scattering parameters of randomly oriented snow particles if radius of equal-volume ice spheres r_{eff} is known over this range. On the other hand, when $x > 2.5$, scattering parameters of nonspherical particles are sensitive to the particle shapes because they are in an anomalous diffraction regime. In this regime, particles have a smaller projected area for a given volume so that the "unfavorable" interference effect grows, resulting in smaller minimum values of scattering cross sections and asymmetry factors. Single scattering parameters averaged over a Gamma size distribution show that scattering coefficients are sensitive to shapes and that differences are larger than 10% when $\pi D_m/\lambda$; the size parameter of the median mass diameter (D_m) is greater than 1. Single scattering albedo values do not show significant differences over most size parameter ranges considered in this study. Asymmetry factors are sensitive to particle shapes when $\pi D_m/\lambda$ is greater than 2.

Citation: Kim, M.-J. (2006), Single scattering parameters of randomly oriented snow particles at microwave frequencies, *J. Geophys. Res.*, *111*, D14201, doi:10.1029/2005JD006892.

1. Introduction

[2] Snowfall is an important part of the Earth's precipitation and hydrological cycle. Heavy snowfall can be disruptive to traffic flows and the economy and the accumulated snow on the ground can cause severe flooding during the following spring. Improved understanding of extratropical precipitation is critical to formulating and verifying methods to realistically capture cycling of water in regional and large-scale climate models. Polar precipitation, mainly as frozen hydrometeors, is an important factor that determines the mass balance of the polar ice sheets. The accumulated snow over land can affect earth energy balance through the surface albedo change. Ground-based radars have been used to monitor the snowfall intensity. However, spatial coverage of radar networks outside of USA, Europe, and Japan is sparse. Snowfall measurement from space can overcome this spatial sampling limit.

[3] Millimeter-wave radiometers operating at frequencies greater than 90 GHz have been employed to estimate frozen hydrometeors [*Chen and Staelin*, 2003; *Kongoli et al.*, 2003; *Skofronick-Jackson et al.*, 2004; *Liu*, 2004; *Kim*, 2004] because of their high sensitivity to scattering by snow in the atmosphere. At these frequencies the Earth's surface features are generally obscured by water vapor in the planetary boundary layer such that they rarely contaminate precipitation signatures from a down-looking spaceborne radiometer. The Special Sensor Microwave/T-2 (SSM/T-2) radiometer and the advanced microwave sounding units (AMSU-B) radiometers on the NOAA 15, 16, and 17 spacecraft provide observations at 89, 150, and 183.3 ± 1, ±3, and ±7 GHz. The forthcoming Global Precipitation Mission (GPM) satellite will include millimeter-wave radiometers to measure snowfall.

[4] Developing physically based algorithms to retrieve snowfall using millimeter-wave radiometers requires computations of brightness temperatures using a radiative trans-

[1]Goddard Earth Science and Technology, University of Maryland, Baltimore County, Baltimore, Maryland, USA.
[2]Department of Atmospheric Sciences, University of Washington, Seattle, Washington, USA.
[3]NASA Goddard Space Flight Center, Greenbelt, Maryland, USA.

0148-0227/06/2005JD006892$09.00

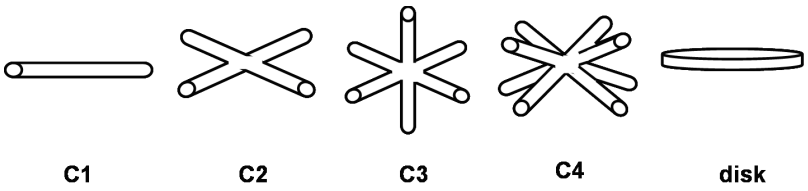

Figure 1. Model crystal habits considered in this study.

fer model. For cloud profiles including frozen precipitation, employing accurate single scattering parameters of nonspherical snow particles in a radiative transfer model is critical. Among the difficulties encountered in calculating single scattering characteristics of nonspherical snow crystals are the unknown distributions of shapes, sizes, orientations, and phase state (i.e., wet snow or dry snow).

[5] This study investigates the effects of nonspherical particle shapes on single scattering parameters. Only dry snow particles are considered in the study. They are assumed to be randomly oriented based on *Vivekanandan et al.* [1994, 1999]. They showed that differential reflectivities to be nearly zero. Differential reflectivity is the ratio of the horizontal copular return to the vertical copular return and can be interpreted as the reflectivity weighted mean axis ratio of the precipitation particle in the radar resolution volume. It is a good indicator of orientation of particles and its near-zero value suggests that snow particles are randomly oriented in dry snow region of precipitating systems.

[6] Single scattering parameters of nonspherical particles can be calculated by solving electromagnetic (EM) equations with rigorous methods like the finite difference time domain (FDTD) [*Yang and Liou*, 1995; *Sun et al.*, 1999], or the discrete dipole approximation (DDA) methods [*Purcell and Pennypacker*, 1973]. However, these methods are computationally expensive. For many physical microwave remote sensing applications to retrieve precipitation, nonspherical frozen hydrometeors have been parameterized as spherical particles. Mie theory is employed because it is faster than the more rigorous methods mentioned above.

[7] One commonly used method approximates the single scattering parameters of nonspherical particles with those of equivalent volume (V) spheres of same density and dielectric constants (hereinafter referred to as equal-V ice spheres). Another popular method used by microwave remote sensing community for precipitation retrievals [*Bauer et al.*, 1999; *Kummerow et al.*, 2001; *Olson et al.*, 2001; *Bennartz and Petty*, 2001] approximates a nonspherical snow crystal as a ''fluffy sphere'' which is a uniform mixture of ice-air [*Meneghini and Liao*, 1996]. Dielectric constants of fluffy spheres are usually determined by mixing formulas [*Maxwell Garnett*, 1904; *Bruggeman*, 1935]. The most commonly used formulas are those of *Maxwell Garnett* [1904] and *Bruggeman* [1935]. For example, TRMM Microwave Imager (TMI) and Special Sensor Microwave Imager (SSM/I) retrieval algorithms, which cover frequencies up to 85 GHz, treat snow crystals as fluffy spherical particles having lower density than pure ice determined by the Maxwell Garnett dielectric mixing formula. They assumed the density of snow crystals of 0.1 g/cm^3 and graupels of 0.4 g/cm^3 [*Bauer et al.*, 1999; *Kummerow et al.*, 2001; *Olson et al.*, 2001]. Recently, *Liu* [2004] showed that the DDA calculated scattering and absorption cross sections and asymmetry parameters of nonspherical snowflakes have values between those of equal-V ice spheres and those of ice-air mixed soft spheres with an effective dielectric constant derived by mixing ice and air using the Maxwell-Garnett formula.

[8] To develop a generally applicable fast and accurate parameterization method to calculate single scattering parameters, requires a thorough understanding of how the snow particle shape affects the scattering parameters at microwave frequencies. This study calculates single scattering parameters of nonspherical snow particles using DDA and T-matrix methods and examines the sensitivity of these parameters to snow particles at microwave frequencies. Single scattering parameters calculated with the DDA method for randomly oriented snow particles are compared with equal-V ice spheres. Some of previous studies [*Liu*, 2004; *O'Brien and Goedecke*, 1988] already showed similar comparisons. However, these studies have not clearly addressed where and why the spherical approximations break down. If spherical approximations can represent the single scattering parameters, computation of scattering parameters can be done more easily by Mie theory. Therefore it is useful to know the upper limit of frequency (or size parameters) where the spherical approximation works. This study shows the range where single scattering parameters are not sensitive to particle shapes and the spherical particle assumptions are valid. DDA computations take large computing effort. We wish that the main results of these calculations tabulated as bench mark values in this paper can be of use for other researchers.

[9] The paper is presented in the following order: Section 2 describes DDA method and the models of nonspherical snow particles. Section 3 compares single scattering parameters calculated with the DDA method. In addition, DDA results of nonspherical snow particles are compared with Mie results of equal-V ice spheres. The sensitivity of single scattering parameters to particle shapes is analyzed. Summary and conclusions are shown in section 4.

2. Computation of Single Scattering Parameters

2.1. Snow Crystal Models

[10] Figure 1 shows five idealized snow crystal models considered in this study: cylindrical columns (C1), and three types of snow aggregates composed of two cylinders (C2), three cylinders (C3) and four cylinders (C4), and disks. The large dimension of particles ranges between 0.06 mm and 5 mm.

[11] Following *Hobbs et al.* [1974], the diameter (D) and length (L) relationship for cylindrical columns considered in this study is given by

$$\ln D = -0.6524 + 1.32 \ln L - 0.0846 (\ln L)^2. \quad (1)$$

The aggregates are modeled with two, three, and four circular cylinders having the same aspect ratio as a single cylindrical column. Disks are assumed to have the same large-small dimension relationship as C1s. Single scattering results for C1s, C2s, C3s, and C4s are analyzed as main snow particle models. Results for disks are employed only to help interpret the sensitivity of scattering properties to particle shape in later part of section 3.

[12] The ice density is assumed to be the same as pure ice. The real (ε') and imaginary (ε'') parts of dielectric constants measured by *Mätzler and Wegmüller* [1987] are employed and are given by

$$\varepsilon' = 3.1884 + 0.00091T \quad (2)$$

$$\varepsilon'' = A/f + Bf^C, \quad (3)$$

where F is frequency (GHz) and T is temperature (°C). They determined that the empirical constants $A = 3.5 \times 10^{-4}$, $B = 3.6 \times 10^{-5}$, $C = 1.2$ at T = −15°C, and $A = 6 \times 10^{-4}$, $B = 6.5 \times 10^{-5}$, $C = 1.07$ at T = −5°C. This study employs equations (2) and (3) for dielectric constants of ice at $T = -15$°C. It can be shown that the dependence of dielectric constants on temperature does not make significant differences (less than 1%) in scattering properties at the frequency range considered in this study.

2.2. Discrete Dipole Approximation Method

[13] The discrete dipole approximation (DDA), which is a flexible technique for calculating the electromagnetic scattering and absorption by particles with arbitrary shapes and composition [*Draine*, 1988; *Mishchenko et al.*, 2000], is employed to calculate the single scattering parameters of C1, C2, C3, and C4 in this study. The DDA treats the actual particle by an array of dipoles. Each of the dipoles is subject to an electric field which is the sum of the incident wave and the electric fields due to all of the other dipoles. Through the solution of the electric field at each dipole position, the scattering and absorption properties of the particle are obtained. The DDA replaces a solid particle with an array of point dipoles occupying positions on a cubic lattice, and the lattice spacing must be small compared to the wavelength of the incident radiation. Therefore the DDA method requires large computer storage and CPU time. The technique is not well suited for particles with very large complex refractive index because it requires much narrower distance between dipoles, thereby requiring much larger memory size. This study employs the DDA codes developed by B. T. Draine and P. J. Flatau (User guide for the Discrete Dipole Approximation Code DDSCAT 6.0, http://arxiv.org/abs/astro-ph/0309069, 2003). Details of the DDA theory are described by *Draine* [1988], *Draine and Flatau* [1994], and *Mishchenko et al.* [2000].

2.3. T-Matrix Method

[14] The T-matrix method pioneered by *Waterman* [1965] can be applied in principal to any arbitrary geometry. The application of the T-matrix method based on the extended boundary condition method for rotationally symmetric shapes [*Wiscombe and Mugnai*, 1986; *Barber and Hill*, 1990; *Mishchenko and Travis*, 1998]. Recently the numerical implementation of this method was extended to geometries other than axisymmetric particles. However, the applicable size parameter region of the T-matrix is usually narrower than for axisymmetric particles. In addition, T-matrix does not generate solutions for particle shapes with extreme aspect ratio [*Mishchenko and Travis*, 1998]. In practice, the analytical approach of T-matrix can substantially speed up numerical computations so that a combination of scattering computational methods, such as the DDA and the FDTD, may shed new light on efficient computation of the single scattering properties of nonspherical particles [*Lee et al.*, 2003]. The T-matrix codes developed by *Mishchenko and Travis* [1998] have limitation to compute scattering parameters of C1s, C2s, C3s, C4s considered in this study because of the extreme aspect ratio for C1s and nonaxisymmetric shapes for C2s, C3s, and C4s. Therefore T-matrix method is used only to compute the single scattering parameters for thick disks in section 3.

3. Results

[15] Figure 2 shows the DDA calculated single scattering properties of randomly oriented snow particles. Scattering cross sections (C_{sca}), absorption cross sections (C_{abs}), and asymmetry factors are plotted against the size parameter $x = 2\pi r_{eff}/\lambda$, where r_{eff} is the radius of equal-V ice spheres and λ is the wavelength. Different symbols represent the DDA results for different shapes of nonspherical snow particles and solid lines represent the Mie calculated results for equal-V ice spheres. Results at different frequencies are coded with different colors. It is clear that DDA calculated scattering cross sections, absorption cross sections, and asymmetry factors of all C1s, C2s, C3s, and C4s overlap with Mie curves when $x \leq 2.5$ at a fixed frequency. This suggests that extinction cross sections and asymmetry factors of randomly oriented snow crystals are not sensitive to the detailed shape of particles and that particles can be assumed as spheres and the Mie solutions can be used when $x \leq 2.5$ at a fixed microwave frequency.

[16] When $x > 2.5$ in Figure 2, Mie curves for spherical particles show ripples caused by surface waves. Results show that the DDA calculated extinction cross sections and asymmetry factors vary depending on particle shapes in this regime. The scattering cross sections and asymmetry factors of nonspherical particles show significantly larger values than Mie solutions. Nonspherical snow particles composed of more number of cylinders show smaller scattering cross sections and asymmetry factors when $x > 2.5$.

[17] Figure 3 shows $C_{sca}/\pi r_{eff}^2$ and $C_{abs}/\pi r_{eff}^2$ of C1s, C2s, C3s, and C4s versus the size parameter $x = \pi D_{eff}/\lambda$. Clearly, the $C_{sca}/\pi r_{eff}^2$ and $C_{abs}/\pi r_{eff}^2$ of C1s, C2s, C3s, and C4s follow the same curve and overlap with Mie curves regardless of how many cylinders compose a snow particle when $x \leq 2.5$. This suggests that each of these parameters is a function of x without much dependence on particle shapes

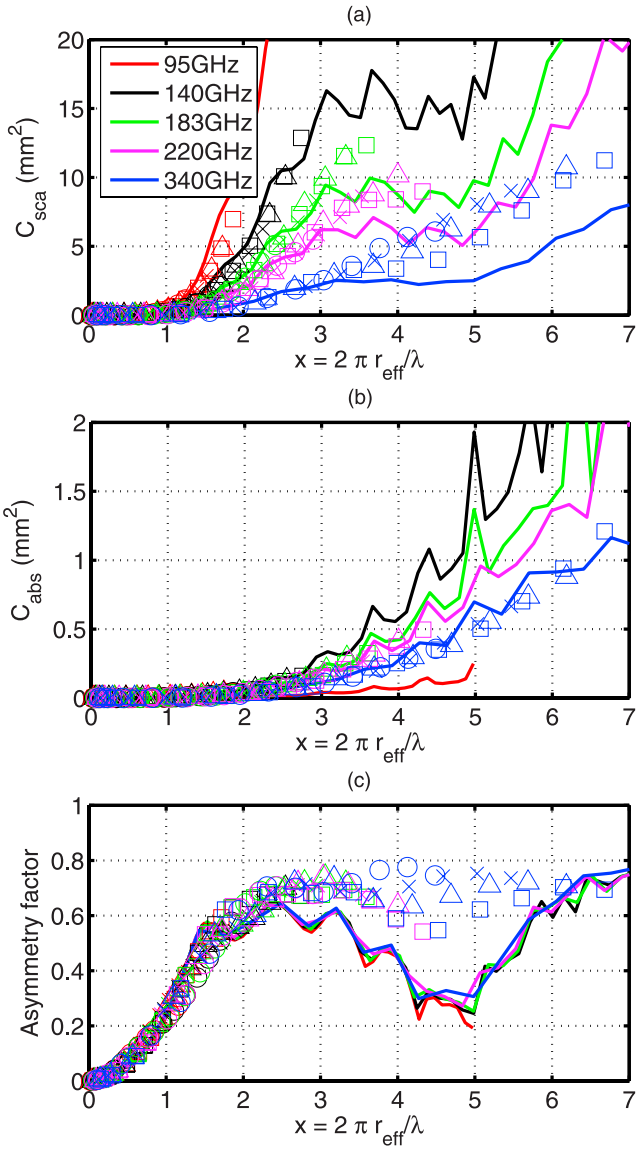

Figure 2. Comparisons of scattering cross sections (C_{sca}), absorption cross sections (C_{abs}), and asymmetry factors for different snow particle models. The x axis shows the size parameter defined as $x = 2\pi r_{eff}/\lambda$, where r_{eff} is the radius of equal-V spheres and λ is the wavelength. Particles are all assumed to be randomly oriented. Solid lines show the Mie calculation results for spheres, and different symbols show the DDA calculated scattering parameters of different particle shapes (open circles, C1; crosses, C2; triangles, C3; squares, C4).

when $x \leq 2.5$. The $C_{sca}/\pi r_{eff}^2$ values show the maximum peak at $x \sim 2.5$. When $x > 2.5$, $C_{sca}/\pi r_{eff}^2$ decreases as size parameter increases and exhibit a significant sensitivity to detailed particle shapes. Spherical particles (shown in solid curves) show the largest decrement and have the minimum $C_{sca}/\pi r_{eff}^2$ values at $x \sim 5$. C1s show larger $C_{sca}/\pi r_{eff}^2$ than C2s, C3s, and C4s.

[18] The criterion $x \sim 2.5$ is explained by the anomalous diffraction theory [*van de Hulst*, 1957, chap. 11]. When x is small and refractive index is near 1, the scattering patterns follow the Rayleigh-Gans approximation so that volume of particles determines the scattering patterns for a given refractive index and for a given wavelength, regardless of the particle shape [*van de Hulst*, 1957]. When x is large and refractive index is near 1, particle scattering is in the anomalous diffraction regime, where the scattered wave intensity is determined by the interferences of transmitted waves and diffracted waves. The phase lag suffered by transmitted waves is determined by the path traveled by the wave in the particle and the intensity distribution in diffraction pattern depends on the projected area (i.e., geometrical shadow) of the particle. Therefore single scattering parameters determined by the combination of transmitted waves and diffracted waves are sensitive to particle shapes in anomalous diffraction regime. *Van de Hulst* [1957] also

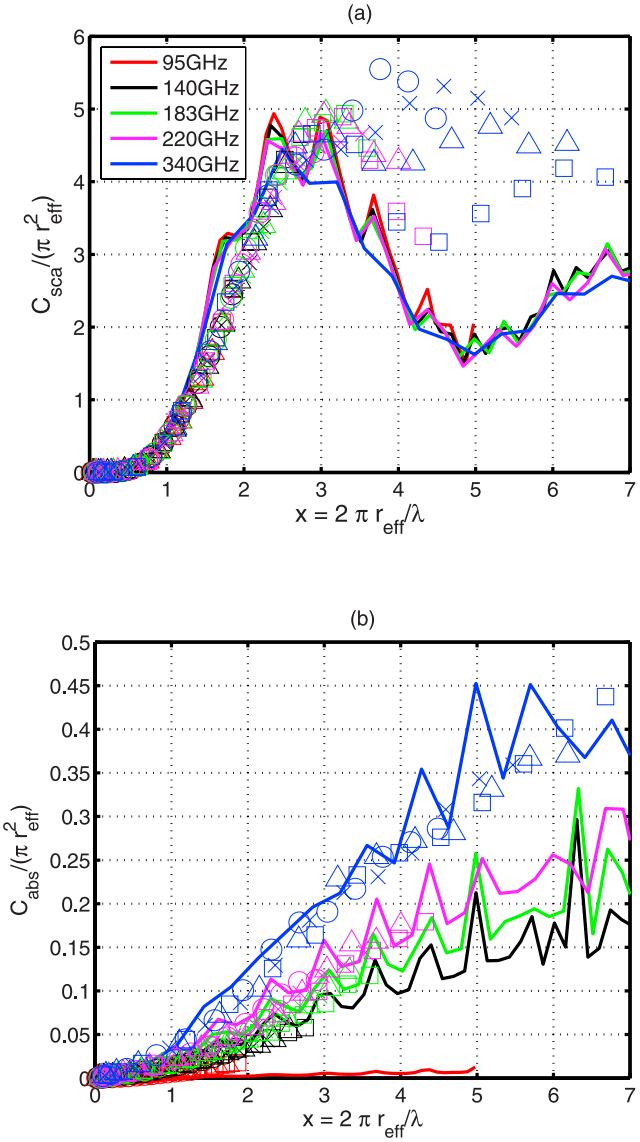

Figure 3. Comparisons of $C_{sca}/\pi r_{eff}^2$ and $C_{abs}/\pi r_{eff}^2$ for different particle shapes. Solid lines show the Mie calculation results for equal-V ice spheres, and different symbols show the DDA calculated scattering parameters of different particle shapes (open circles, C1; crosses, C2; triangles, C3; squares, C4).

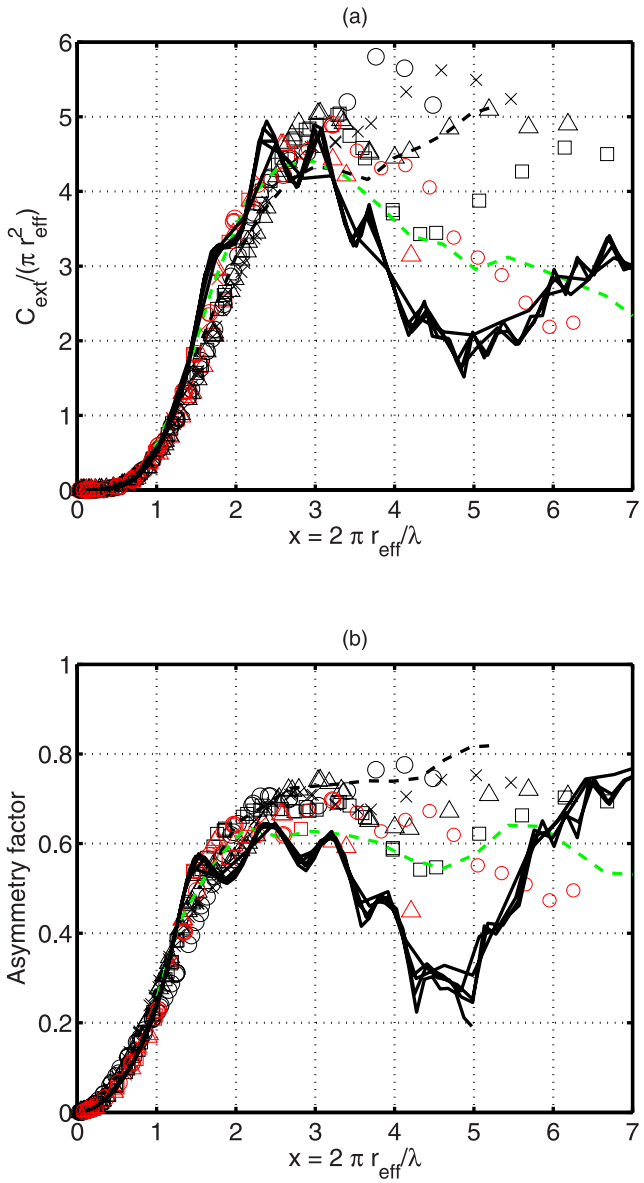

Figure 4. Comparisons of $C_{ext}/\pi r_{eff}^2$ and asymmetry factors for different particle shapes. Solid lines show the Mie calculation results for spheres at various frequencies. Black and green dashed lines show the results of thin and thick disks, respectively. Black (red) colored symbols show the DDA calculated scattering parameters of thin (thick) C1s, C2s, C3s, and C4s (open circles, C1; crosses, C2; triangles, C3; squares, C4).

shows that the first maxima of extinction efficiency of spherical particles and cylindrical particles occur at $x = 2 \sim 2.5$ in the anomalous diffraction regime [see *van de Hulst*, 1957, Figures 32 and 65, Table 15]. The existence of maxima and minima in intensity of scattered wave (Q_{ext}) are caused by the "favorable" and "unfavorable" interferences, respectively.

[19] To examine the sensitivity of particle scattering to the thickness of component cylinders, single scattering parameters are calculated with the DDA method for snow particles composed of one, two, three, and four cylinders with double the thickness of C1s (hereinafter referred to as thickC1, thickC2, thickC3, and thickC4). In addition, single scattering parameters of disks, which have the same small-large dimension relationships as C1s and thickC1s, are calculated with T-matrix methods [*Mishchenko et al.*, 1996]. Hereinafter, they are referred to as "thin" disks and "thick" disks, respectively. The results are plotted in Figure 4, where the $C_{ext}/\pi r_{eff}^2$ and asymmetry factors of C1s, C2s, C3s, C4s, thickC1s, thickC2s, thickC3s, thickC4s, and thin and thick disks are compared. Here C_{ext} (= C_{abs} + C_{sca}) is the extinction cross section. Black symbols present the results of C1s, C2s, C3s, and C4s and red symbols present results of thickC1s, thickC2s, thickC3s, and thickC4s. Overlapped solid lines show the Mie curves at different frequencies. Overlapped dashed lines show the results of randomly oriented thin disks and thick disks.

[20] When $x \leq 2.5$, thickC1s, thickC2s, thickC3s, thickC4s and thick disks show more consistent $C_{ext}/\pi r_{eff}^2$ values with those of the spherical particles than C1s, C2s, C3s, and C4s and thin disks. Thick disks are well overlapped with thickC1s, thickC2s, thickC3s, thickC4s while thin disks are well overlapped with C1s, C2s, C3s, and C4s. This suggests that $C_{ext}/\pi r_{eff}^2$ of randomly oriented nonspherical particles are dependent on the small dimensions of components for a given volume. Asymmetry factors of all particle shapes considered in this study (i.e., spheres, C1s, C2s, C3s, C4s, thickC1s, thickC2s, thickC3s, thickC4s, thick disks, and thin disks) are nearly overlapping with one another. This suggests that the asymmetry factors of ice particles are mostly determined by the size of particles and not by shapes of particles when $x \leq 2.5$.

[21] When $x > 2.5$, extinction cross sections and asymmetry factors of nonspherical particles are sensitive to the particle shapes. Figure 4 suggests that spherical particles suffer unfavorable interferences most while C1s suffer unfavorable interferences least among particle considered in this study. That is because particles with smaller projected area for a given volume have larger phase lags suffered by the transmitted waves so that unfavorable interferences grow. Thick disks and thick cylinders, which have similar projected area for a given volume, show relatively consistent $C_{ext}/\pi r_{eff}^2$ and asymmetry factors with each other. However, spheres show relatively small $C_{ext}/\pi r_{eff}^2$ and asymmetry factors because they relatively large suffer unfavorable interferences. Thin disks and thin cylinders show relatively large $C_{ext}/\pi r_{eff}^2$ and asymmetry factors because they suffer relatively small unfavorable interferences.

[22] To facilitate the use of these calculated scattering parameters, curve fitting is applied to the data in the above

Table 1. Fitting Coefficients for the Scattering Cross Sections

	C1	C2	C3	C4
A_0	−0.3353	−0.3533	−0.3597	−0.3432
A_1	3.3177	3.3295	3.3643	3.4542
A_2	−1.7217	−1.6769	−1.5013	−1.4338
A_3	−1.7254	−1.9710	−2.0822	−2.6021
A_4	−0.1953	−0.5256	−1.2714	−2.2706
A_5	0.7358	1.1379	0.9382	1.1111
A_6	0.4084	1.1043	1.6981	2.8529
A_7	0.0554	0.2963	0.6088	1.1258

Table 2. Fitting Coefficients for the Absorption Cross Sections

	95 GHz	140 GHz	183 GHz	220 GHz	340 GHz
B_0	1.508E-04	1.122E-04	-6.598E-04	0.0019	0.0063
B_1	0.0021	0.0061	0.0153	8.275E-04	−0.0145
B_2	0.0081	0.0086	−0.0032	0.0189	0.0502
B_3	−0.0051	−0.0022	0.0062	−0.0022	−0.0105
B_4	0.002	5.35E-04	−0.0014	−4.49E-05	6.998E-04
B_5	−2.596E-04	−4.82E-05	8.49E-05	1.24E-05	8.68E-07

figures. Tables 1, 2, and 3 show the fitting coefficients for the following functions relating scattering cross sections ($C_{sca}/\pi r_{reff}^2$), absorption cross sections ($C_{sca}/\pi r_{reff}^2$), and asymmetry factors (g) calculated in this study to the size parameters $x = 2\pi r_{eff}/\lambda$. Where r_{eff} is the radius of equal-V ice spheres and λ is the wavelength. The C1, C2, C3, and C4 in the tables refer to the snow crystal models shown in Figure 1:

$$\log_{10}\left(\frac{C_{sca}}{\pi r_{eff}^2}\right) = \sum_{n=0}^{7} A_n (\log_{10} x)^n, \tag{4}$$

$$\frac{C_{abs}}{\pi r_{eff}^2} = \sum_{n=0}^{5} B_n x^n, \tag{5}$$

$$\log_{10}(g) = \sum_{n=0}^{7} F_n (\log_{10} x)^n. \tag{6}$$

[23] To examine the sensitivity of scattering properties to particle shapes after averaging over particle size distributions, fitting functions shown in equations (4), (5), and (6) are employed to calculate the scattering coefficients (k_{sca}), single scattering albedo ($\overline{\omega}$), and asymmetry factors ($\overline{g}$):

$$k_{sca} = \int_{D_{min}}^{D_{max}} C_{sca}(D) N(D) dD, \tag{7}$$

$$k_{abs} = \int_{D_{min}}^{D_{max}} C_{abs}(D) N(D) dD, \tag{8}$$

$$\overline{g} = \frac{1}{k_{sca}} \int_{D_{min}}^{D_{max}} g(D) C_{sca}(D) N(D) dD, \tag{9}$$

Table 3. Fitting Coefficients for the Asymmetry Factors

				C4	
	C1	C2	C3	$x < 1$	$x \geq 1$
F_0	−0.6304	−0.5673	−0.5832	−0.6122	−0.4654
F_1	1.5281	1.5418	1.6818	2.3329	−3.9724
F_2	−0.2125	−1.0410	−1.0855	3.6036	81.0301
F_3	−0.9502	−1.0442	−1.4262	13.9784	−504.904
F_4	−1.7090	−0.0600	−0.2155	26.3336	1569.3
F_5	0.1557	0.8422	1.0944	26.3125	−2620.1
F_6	1.4016	0.6686	0.8690	13.4166	2230.9
F_7	0.5477	0.1597	0.1937	2.7443	−757.586

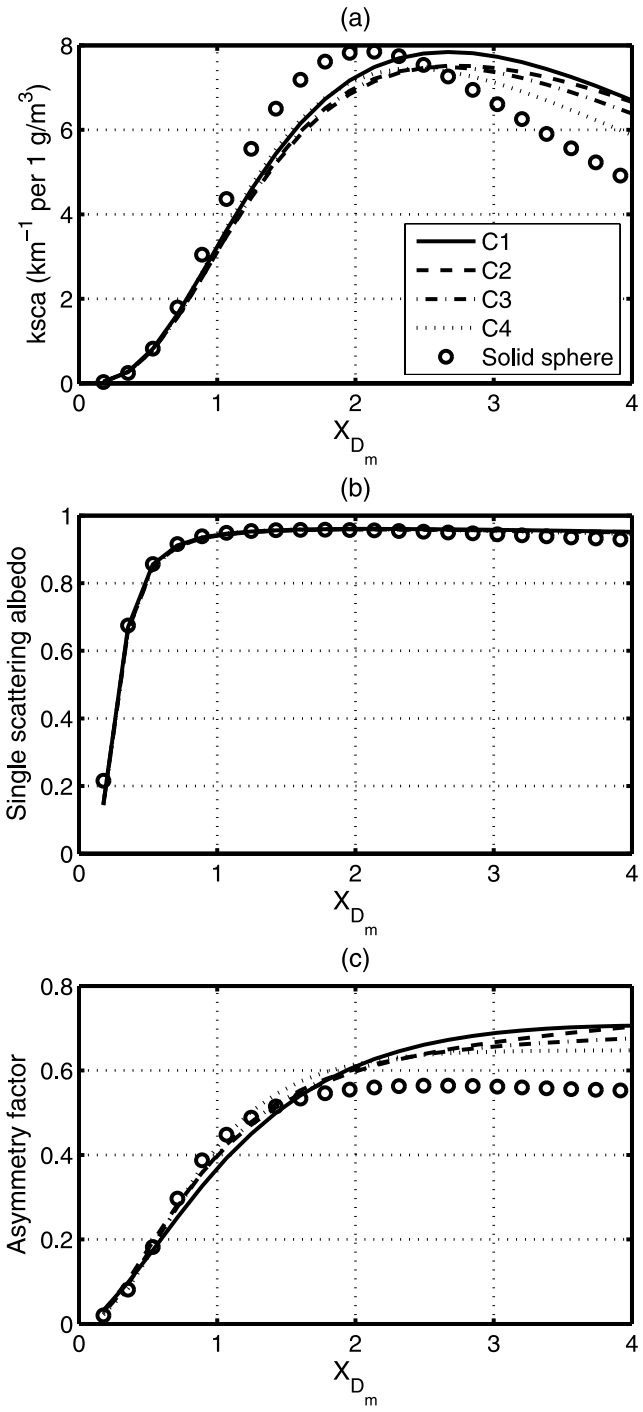

Figure 5. Single-scattering parameters averaged over a Gamma size distribution (equation (4)) with $\mu = 2$. Mie results for solid spheres are shown for comparison.

$$\overline{\omega} = \frac{k_{sca}}{k_{sca} + k_{abs}}. \tag{10}$$

Here $N(D)$ is the Gamma particle size distribution defined by

$$N(D) = N_0 D^{\mu} \exp(-\Lambda D), \tag{11}$$

where $\Lambda = \mu + 3.67/D_m$ and D_m is the mass-weighted mean diameter.

[24] Figure 5 shows single scattering parameters averaged over Gamma size distributions with $\mu = 2$ and with various D_m, plotted against size parameter $x_{D_m} = \pi D_m/\lambda$. The $D_{\min}$, $D_{\max}$, and dD values used in the integrations (equations (7)–(9)) are 0.01 mm, 3.6 mm, and 0.01 mm, respectively. Mie results for solid spheres are included in the figure for comparisons. Results show that scattering coefficients are sensitive to shapes of particles, difference being larger than 10% when $x_{D_m} > 1$. Scattering coefficients of spherical particles are larger than those of nonspherical particles when $x_{D_m} < 2$ and decrease after the maximum peak at $x_{D_m} \approx 2$. When $x_{D_m} > 2.5$, C1s give the largest scattering coefficients and spheres the smallest. Single scattering albedo values do not show significant differences over most of x_{D_m} ranges considered in this study. Asymmetry factors are sensitive to particle shapes when $x_{D_m} > 2$. For example, asymmetry factors of C1s are larger than those of spheres by 20% when $x_{D_m} = 3$.

4. Conclusions and Discussions

[25] The discrete dipole approximation (DDA) method and the T-matrix method are used to calculate single scattering parameters (scattering cross sections, absorption cross sections, and asymmetry factors) of various nonspherical snow particles at microwave frequencies between 95 GHz and 340 GHz. Results of these calculations are used to examine the sensitivity of single scattering parameters to nonspherical particle shapes. It is shown that scattering cross sections, absorption cross sections, and asymmetry factors of complex particles at a fixed frequency are insensitive to particle shapes when the size parameter $x = 2\pi r_{\text{eff}}/\lambda$ is less than about 2.5 where r_{eff} is the radius of equal-volume (V) ice spheres. In addition, results show that $C_{\text{sca}}/\pi r_{\text{eff}}^2$ and asymmetry factors are functions of x, respectively, without much dependence on particle shapes when $x \leq 2.5$. Mie theory may be used to compute the single scattering parameters of randomly oriented snow particles if equal-V diameter, r_{eff} is known over this range of size parameter.

[26] However, when $x > 2.5$, scattering parameters of nonspherical particles are sensitive to the particle shapes because scattering occurs in an anomalous diffraction regime. In this regime, distributions of scattered wave intensity are determined by the interferences of transmitted waves and diffracted waves. Because the phase lag suffered by transmitted waves is determined by the path traveled by the wave in the particle and the intensity distribution in diffraction pattern depends on the projected area (i.e., geometrical shadow) of the particle [*van de Hulst*, 1957]. Therefore single scattering parameters are sensitive to particle shapes.

[27] Single scattering parameters averaged over a Gamma size distribution show that scattering coefficients are sensitive to shapes and the differences are larger than 10% when size parameter of median mass diameter (D_m) is greater than 1. Single scattering albedo values do not show significant differences over most of size parameter ranges considered in this study. Asymmetry factors are sensitive to particle shapes when size parameter of median mass diameter (D_m) is greater than 2.

[28] **Acknowledgments.** The author thanks James Wang, James Weinman, and Robert Meneghini for their constructive comments on this paper. Draine and Flatau kindly provided the author with the DDSCAT codes. Interest in our work by Ramesh Kakar of Code Y at NASA HQ and support from the Goddard Director's Discretionary Fund are also acknowledged. This work has been supported by NASA grants NCC-5-584, S-69019-G, and NAG5-9668.

References

Barber, P. W., and S. C. Hill (1990), *Light Scattering by Particles: Computational Methods*, World Sci., Singapore.

Bauer, P., J. P. V. Poiares Baptista, and M. de Iulis (1999), The effect of the melting layer on the microwave emission of clouds over the ocean, *J. Atmos. Sci.*, *56*, 852–867.

Bennartz, R., and G. W. Petty (2001), The sensitivity of microwave remote sensing observations of precipitation to ice particle size distributions, *J. Appl. Meteorol.*, *40*, 345–364.

Bruggeman, D. A. G. (1935), Berechung verschiedener physikalischer Konstanten von heterogenen Substanzen, *Ann. Phys.*, *24*, 646–679.

Chen, F. W., and D. H. Staelin (2003), AIRS/AMSU/HSB precipitation estimates, *IEEE Trans. Geosci. Remote Sens.*, *4*, 410–417.

Draine, B. T. (1988), The discrete dipole approximation and its application to interstellar graphite grains, *Astrophys. J.*, *333*, 848–872.

Draine, B. T., and P. J. Flatau (1994), Discrete dipole approximation for scattering calculations, *J. Opt. Soc. Am.*, *A11*, 1491.

Hobbs, P. V., S. Chang, and J. D. Locatelli (1974), The dimensions and aggregation of ice crystals in natural clouds, *J. Geophys. Res.*, *79*, 2199–2206.

Kim, M.-J. (2004), A physical model to estimate snowfall over land using microwave measurements, Ph.D. thesis, 151 pp., Atmos. Sci. Dep., Univ. of Wash., Seattle.

Kongoli, C., P. Pellegrino, R. Ferraro, N. Grody, and H. Meng (2003), A new snowfall detection algorithm over land using measurements from the Advanced Microwave Sounding Unit (AMSU), *Geophys. Res. Lett.*, *30*(14), 1756, doi:10.1029/2003GL017177.

Kummerow, C., Y. Hong, W. S. Olson, S. Yang, R. F. Adler, J. McCollum, R. Ferraro, G. Petty, D.-B. Shin, and T. T. Wilheit (2001), The evolution of the Goddard Profiling Algorithm (GPROF) for rainfall estimation from passive microwave sensors, *J. Appl. Meteorol.*, *40*, 1801–1820.

Lee, Y.-K., M. I. Mishchenko, B. A. Baum, Y. X. Hu, H.-L. Huang, W. J. Wiscombe, and A. J. Baran (2003), Use of circular cylinders as surrogates for hexagonal pristine ice crystals in scattering calculations at infrared wavelengths, *Appl. Opt.*, *42*, 2653–2664.

Liu, G. (2004), Approximation of single scattering properties of ice and snow particles for high microwave frequencies, *J. Atmos. Sci.*, *61*, 2441–2456.

Mätzler, C., and U. Wegmüller (1987), Dielectric properties of fresh-water ice at microwave frequencies, *J. Phys. D Appl. Phys.*, *20*, 1623–1630.

Maxwell Garnett, J. C. (1904), Colours in metal glasses and in metallic films, *Philos. Trans. R. Soc. London, Ser. A*, *203*, 385–420.

Meneghini, R., and L. Liao (1996), Comparisons of cross sections for melting hydrometeors as derived from dielectric mixing formulas and a numerical method, *J. Appl. Meteorol.*, *35*, 1658–1670.

Mishchenko, M. I., and L. D. Travis (1998), Capabilities and limitations of a current FORTRAN implementation of the T-matrix method for randomly oriented, rotationally symmetric scatters, *J. Quant. Spectrosc. Radiat. Transfer*, *60*, 309–324.

Mishchenko, M. I., L. D. Travis, and D. W. Mackowski (1996), T-matrix computations of light scattering by nonspherical particles: A review, *J. Quant. Spectrosc. Radiat. Transfer*, *55*, 535–575.

Mishchenko, M. I., J. W. Hovenier, and L. D. Travis (2000), *Light Scattering by Nonspherical Particles*, 690 pp., Elsevier, New York.

O'Brien, S. G., and G. H. Goedecke (1988), Scattering of millimeter waves by snow crystals and equivalent homogeneous symmetric particles, *Appl. Opt.*, *27*, 2439–2444.

Olson, W., P. Bauer, N. F. Viltard, D. E. Johnson, W.-K. Tao, R. Meneghini, and L. Liao (2001), A melting-layer model for passive/active microwave remote sensing applications. part I: Model formulation and comparison with observations, *J. Appl. Meteorol.*, *40*, 1145–1163.

Purcell, E. M., and C. R. Pennypacker (1973), Scattering and absorption of light by nonspherical diectric grains, *Astrophys. J.*, *186*, 705–714.

Skofronick-Jackson, G. M., M.-J. Kim, J. A. Weinman, and D.-E. Chang (2004), A physical model to determine snowfall over land by microwave radiometry, *IEEE Trans. Geosci. Remote Sens.*, *42*, 1047–1058.

Sun, W., Q. Fu, and Z. Z. Chen (1999), Finite-difference time domain solution of light scattering by dielectric particles with a perfectly matched layer absorbing boundary condition, *Appl. Opt.*, *38*, 3141–3151.

van de Hulst, H. C. (1957), *Light Scattering by Small Particles*, 470 pp., Dover, Mineola, N. Y.

Vivekanandan, J., V. N. Bringi, M. Hagen, and P. Meischner (1994), Polarimetric radar studies of atmospheric ice particles, *IEEE Trans. Geosci. Remote Sens.*, *32*, 1–10.

Vivekanandan, J., S. M. Ellis, R. Oye, D. S. Zrnic, A. V. Ryzhkov, and J. Straka (1999), Cloud microphysics retrieval using S-band dual-polarization radar measurements, *Bull. Am. Meteorol. Soc.*, *80*, 381–388.

Waterman, P. C. (1965), Matrix formulation of electromagnetic scattering, *Proc. IEEE*, *53*, 805–812.

Wiscombe, W. J., and A. Mugnai (1986), Scattering from nonspherical Chebyshev particles. 2. Means of angular scattering patterns, *Appl. Opt.*, *27*, 2405–2421.

Yang, P., and K. N. Liou (1995), Light scattering by hexagonal ice crystals: Comparison of finite-difference time domain and geometric optics models, *J. Opt. Soc. Am. A Opt. Image Sci.*, *12*, 162–176.

M.-J. Kim, NASA Goddard Space Flight Center, Mail Code 614.6, Greenbelt, MD 20771, USA. (mjkim@neptune.gsfc.nasa.gov)